Article

Controllable Fabrication of Organic Cocrystals with Interior Hollow Structure Based on Donor-Acceptor Charge Transfer Molecules

Yuhao Li, Peiyao Wang, Zhongzhao Duan, Tianle Zhang and Fei Tong *

Key Laboratory for Advanced Materials and Joint International Research Laboratory of Precision Chemistry and Molecular Engineering, Feringa Nobel Prize Scientist Joint Research Center, Frontiers Science Center for Materiobilogy and Dynamic Chemistry, Institute of Fine Chemicals, School of Chemistry and Molecular Engineering, East China University of Science and Technology, Shanghai 200237, China
* Correspondence: feitong@ecust.edu.cn

Abstract: Fluorescent hollow organic molecular cocrystals comprised of (E)-4-(2(anthracen-9-yl)vinyl) pyridine-1,2,4,5-tetracyanobenzene (APE-TCNB) were prepared via a surfactant-mediated co-precipitation method. The size and morphology of these cocrystals could be easily tuned by varying the type and concentration of the surfactant, incubation time, and temperature. Moreover, optical fluorescence and scanning electron microscopy characterization indicated that the APE-TCNB microcrystals contained two symmetric empty cavities when 3-(N, N-dimethyldodecylammonio)propane sulfonate (BS12) was used as the surfactant. The cross-polarized microscope and powder X-ray diffraction (PXRD) measurements both showed that the prepared microcrystals exhibited high crystallinity. APE and TCNB molecules were found to align parallelly along the crystallographic a-axis in the crystal lattice, and the strong π–π intermolecular interactions facilitated the formation of unique crystal chambers. A series of measurements and characterization, including UV-Vis absorption spectroscopy, infrared spectroscopy, steady-state, and time-resolved fluorescence spectroscopy, also verified that strong charge–transfer (CT) interactions had been established in the APE-TCNB microcrystals. Moreover, these APE-TCNB microcrystals could emit bright red luminescence, which extended to the near-infrared region (~800 nm), displaying a strong charge-transfer property. Here, we have shown a general facile way to make organic cocrystals with complex structures and topologies using a self-assembly method.

Keywords: organic molecular cocrystal; self-assembly; π–π interactions; hollow structure

1. Introduction

Organic molecular crystals with novel electronic, photophysical, and mechanical properties have inspired great interest because of their unique chemical structures and highly ordered arrays [1–4]. Except for intrinsic factors such as molecular and crystal structures, size, shape, and morphology can also profoundly influence the properties of a crystal [5–8]. Classic crystal growth methods such as sublimation and solution recrystallization usually result in different crystal shapes and a wide crystal size distribution [9–11]. Therefore, numerous techniques have been adopted to achieve various crystal morphologies and shapes [12–15]. However, engineering more sophisticated morphologies for organic crystals remains to be challenging as the weak intermolecular interactions usually make it difficult to regulate the desired crystal shape and size. Instead of traditional crystal methods, the solution self-assembly method offers a facile strategy to construct molecular crystals with specific morphologies and structures [16–18]. Bardeen and Al-Kaysi pioneered this strategy by combining surfactant and solvent exchange methods to prepare various photomechanical molecular crystals, including microblocks, microplates, microwires, and octahedron microcrystals, which could exhibit various photomechanical responses [19–22].

The self-assembly method offers an effective and fast way to make molecular crystals with different shapes and sizes from solutions. Moreover, it has been reported that complicated crystal topologies, such as unique tubular and hollow structures, could be obtained during crystal growth by regulating intermolecular interactions such as π–π interactions [23–26].

Cocrystal engineering or cocrystallization through a self-assembly method that stacks different organic molecules in an ordered way with a specific stoichiometric ratio of each component provides an effective approach for fabricating new hybrid molecular crystals with multiple functions [27–29]. The crystal structure of a cocrystal can be adjusted by changing the stoichiometric ratio of starting materials, resulting in different properties. It is possible for a cocrystal to either combine all advantages of each constituent or generate new superior properties [30–32]. Therefore, cocrystals continue to draw increasing interest nowadays, even though the concept was established over a hundred years ago [33]. To date, methods of making cocrystals capable of exhibiting potential applications for dyes, pigments, pharmaceuticals, and optoelectronics have been extensively explored and developed [34–36].

Herein, we used a surfactant-mediated co-reprecipitation way to grow a new type of charge-transfer (CT) cocrystal that consists of (*E*)-4-(2(anthracen-9-yl)vinyl)pyridine (APE) and 1,2,4,5-tetracyanobenzene (TCNB). APE possesses a molecular structure in which anthracene and pyridine rings are the aromatic frameworks that allow for strong π–π interactions. In addition, the APE molecule also has remarkable luminescence properties, which facilitate the characterization of cocrystals. Regular rectangular microcrystals with a relatively narrow distribution of crystal size were obtained. Crystal size and morphology could be tuned by varying the surfactant concentration and the incubation temperature. In addition, cocrystals that contained two symmetric hollow cavities could be fabricated, characterized by optical fluorescence microscope and high-resolution electron microscopes. The powder X-ray diffraction measurements and crossed-polarized microscope both showed that the prepared microcrystals exhibited high crystallinity. Furthermore, the APE-TCNB cocrystals could emit bright red luminescence upon 405 nm light excitation. In addition, the prepared APE-TCNB were thermally stable for several months under an ambient environment and could remain intact after 30 min intense sonication. Our results provide an effective way to make organic cocrystals with complicated topologies and emitting bright luminescence, which can also be engineered to endow more functionalities in the future.

2. Materials and Methods

All starting materials were purchased from J&K Scientific Company and used without further purification. The 3-(N, N-dimethyldodecylammonio)propane sulfonate (BS12) and sodium dodecyl sulfate (SDS) were purchased from Sigma-Aldrich (≥99%). The organic solvents were of analytical reagent grade (AR), and Milli-Q water (18 MΩ/cm) was used throughout the experiments. More detailed information on material synthesis can be found in the Supporting Materials Information.

2.1. Syntheses of (E)-4-(2(anthracen-9-yl)vinyl)pyridine (APE)

The synthetic routes for the APE molecule are shown in Supplementary Figure S1. Specifically, 9-bromoanthracene (2.0 g, 7.9 mmol), K_2CO_3 (3.2 g, 23.2 mmol), PPh$_3$ (306 mg, 1.2 mmol), and Pd(OAc)$_2$ (90 mg, 0.4 mmol) were added in an oven-dried 50 mL Schlenk tube. After the system was sealed and evacuated, dry N, N-dimethylformamide (DMF, General-Reagent, 99.5%) (20 mL), and 4-vinylpyridine (1.2 g, 1,3 mL, 11.6 mmol) were injected into the mixture. Then, the mixture was stirred under Ar at 110 °C for 24 h. The reaction mixture was poured into a LiCl solution (5% wt in 100 mL H_2O), and the suspension was extracted with EtOAc. The combined organic layer was washed by brine for three times, dried over anhydrous $MgSO_4$, and concentrated in vacuo. The crude product was purified by using column chromatography (PE: EtOAc, 3:1), and a bright yellow powder (750 mg, isolated yield = 35%) was collected (Figure S1). ^{1}H NMR (400 MHz, DMSO-d_6): δ 7.00 (d, J = 16 Hz, 1H), 7.54–7.59 (m, 4H), 7.80–7.82 (m, 2H), 8.09–8.16 (m,

2H), 8.32–8.35 (m, 2H), 8.43–8.47 (d, J = 16 Hz, 1H), and 8.63–8.66 (m, 3H) (Figure S2). ^{13}C NMR (600 MHz, DMSO-d_6): δ 121.67, 125.95, 126.63 127.43, 129.19, 129.44, 130.06, 131.50, 131.86, 135.21, 144.42, and 150.60 (Figure S3). HR-MS (EI): Calculated for $C_{21}H_{15}N$, [M^+] = 281.1213, found = 281.1215 (Figure S4).

2.2. Preparation of APE-TCNB Single-Crystals for Structure Determination

First, 28.1 mg APE and 17.8 mg TCNB solid powders were dissolved into 200 μL dry DMF to form a 0.5 M homogenous solution. The solution was placed in an open sample bottle at room temperature. After the solvent fully evaporated (~72 h), APE-TCNB single crystals for structure determination were harvested.

2.3. Preparation of APE-TCNB Hollow Microcrystals Preparation

First, 3.1 mg APE and 2.0 mg TCNB solid powders were separately dissolved into 50 μL dry DMF to form a 0.22 M homogenous solution. APE and TCNB solutions were injected into 10 mL of aqueous surfactant solutions in a water bath (~47 °C). After several seconds of vigorous stirring, the two surfactant solutions were mixed and subjected to multiple cycles of being poured back and forth between different vials. Finally, the mixed solution was placed in an oven set at 47 °C for 2–4 h incubation. After the incubation, microcrystals with hollow chambers were harvested.

2.4. Measurements and Characterization

The ^{1}H NMR and ^{13}C NMR data were both collected from a superconducting Fourier NMR spectrometer (Avance III 400, 400 MHz, Brucker), using deuterated dimethyl sulfoxide-d_6 (DMSO-d_6) as solvent at 373 K. High-resolution time-of-flight mass spectrometry (HR-ESI) was performed using an LCT Premier XE mass spectrometer from the Water Company of the United States. Steady-state absorption, excitation and emission spectra were recorded on a Shimadzu RF-6000 spectrophotometer. The infrared spectroscopy (IR) were collected from a Fourier transform-infrared spectrometer from Thermo Nicolet Corporation of the United States. The optical microscopy measurements were conducted using a Leica DM750 microscope equipped with a QTF500 digital camera. The microscopy fluorescence measurements were performed using a TL-3201LED fluorescence microscope (equipped with a 20MP USB 3.0 digital camera). All PXRD data were collected on an X-ray powder diffractometer (Rigaku, 18 kW/D/Max2550VB/PC, CuKα radiation, λ = 1.5418 Å, 40 kV/100 mA power) at room temperature. The melting point of the APE-TCNB cocrystals was measured using a melting point apparatus (X4-B, Shanghai BM Optical Instrument Manufacturing Company). Specifically, approximately 1 mg of cocrystal powders was placed under an optical microscope connected to the melting point apparatus. When the cocrystal started transforming to a liquid phase, a melting point (~216 °C) was recorded from the apparatus.

3. Results and Discussion

Figure 1 shows the molecules that we used in this work. (*E*)-4-(2(anthracen-9-yl)vinyl) pyridine (APE) that consists of an anthracene backbone and a pyridyl tail was synthesized for the donor molecule, and 1,2,4,5-tetracyanobenzene (TCNB) was used as the typical electron acceptor. The single crystal structure of the APE-TCNB cocrystals that were prepared using a traditional solvent evaporation method is shown in Figure 1b and Table S1, exhibiting strong CT interactions between APE and TCNB molecules. Regarding the APE-TCNB microcrystal preparation, we used surfactant to regulate crystal shape during self-assembly. Specifically, TCNB and APE compounds were first dissolved in N, N-dimethylformamide (N, N-DMF) to form highly concentrated solutions (0.22 M). Then, the solutions were separately injected into aqueous surfactant solutions sitting in a water bath (~47 °C). After a short period of vigorous stirring (stirring rate 1000 rpm), these two aqueous solutions were rapidly mixed to obtain charge-transfer (CT) cocrystals. The mixed solution was poured back and forth between different glass vials to allow the mixture to

become homogenous before being put in an oven for further incubation. After 2–4 h of incubation, rectangular-shaped microcrystals could be harvested.
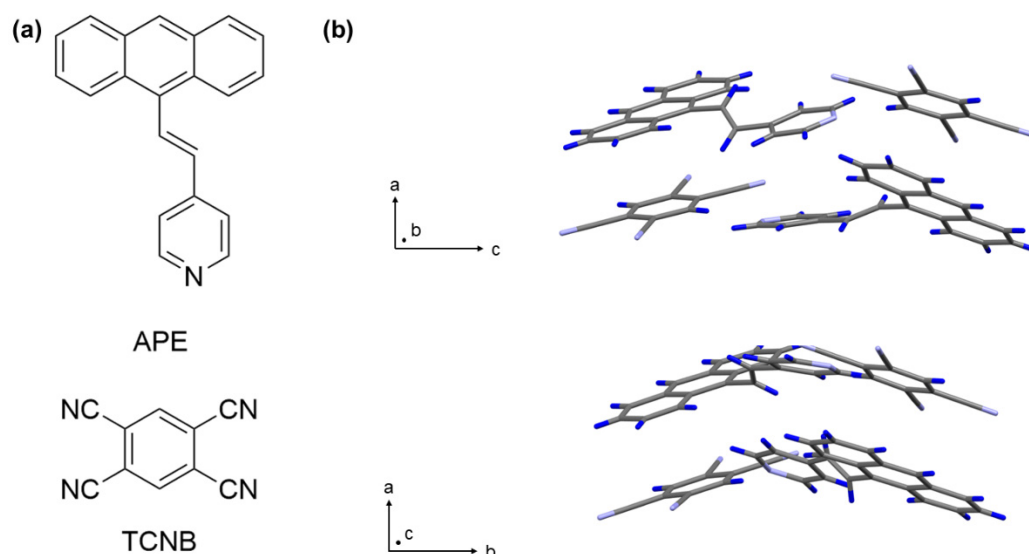

Figure 1. (**a**) Molecular structures used in this work; (**b**) crystal structure of APE-TCNB viewed along the crystallographic *b*-(up) and *c*-(down) axes.

The average size of the prepared microcrystals could be tuned by varying the incubation temperature (37–57 °C), stirring rate, the concentration of surfactant, and the number of mixing cycles. As shown in Table 1, the relationship and the abovementioned factors and crystal morphology and size are listed. The size and morphology of APE-TCNB cocrystal would also differ when different surfactant was used. The APE-TCNB cocrystals prepared in the BS12 solutions have twinned symmetric interior cavities. These hollow APE-TCNB cocrystals can reach up to 100 μm in length and 10 μm in width, and the thickness of the hollow cocrystals ranges from 0.5–1.5 μm (Figure 2a,b). The hollow microcrystals have relatively narrow size distributions, and the interior cavities are empty interior and closed exterior as determined by scanning electron microscopy (SEM) (Figure 2c,d). High-voltage electron beams from SEM could damage the crystal and break the interior cavities (Figure 2d). The punctured crystal cavities also allow us to observe the exterior cover layer, approximately 100 nm (Figure 2d). Therefore, we can estimate the crystal cavity volume by regarding a hollow chamber as a triangular prism. We can assume a length of 30 μm, a depth of 1 μm, and a width of 10 μm. Then, we can calculate that the volume of each hollow cavity is approximately 150 μm^3 and that each hollow APE-TCNB cocrystal contains an empty interior space of about 3×10^{-10} mL. This estimation is based on a large cocrystal with a total length of 100 μm, while smaller cocrystals should possess smaller cavity volumes accordingly. We found that only these cocrystal structures could be obtained by using BS12 surfactant. The APE-TCNB cocrystals grown in SDS solutions are solid cuboids whose length and width can reach up to 100 μm and 10 μm (Figure 3).

Table 1. The influence of surfactant type and temperature on crystal morphology.

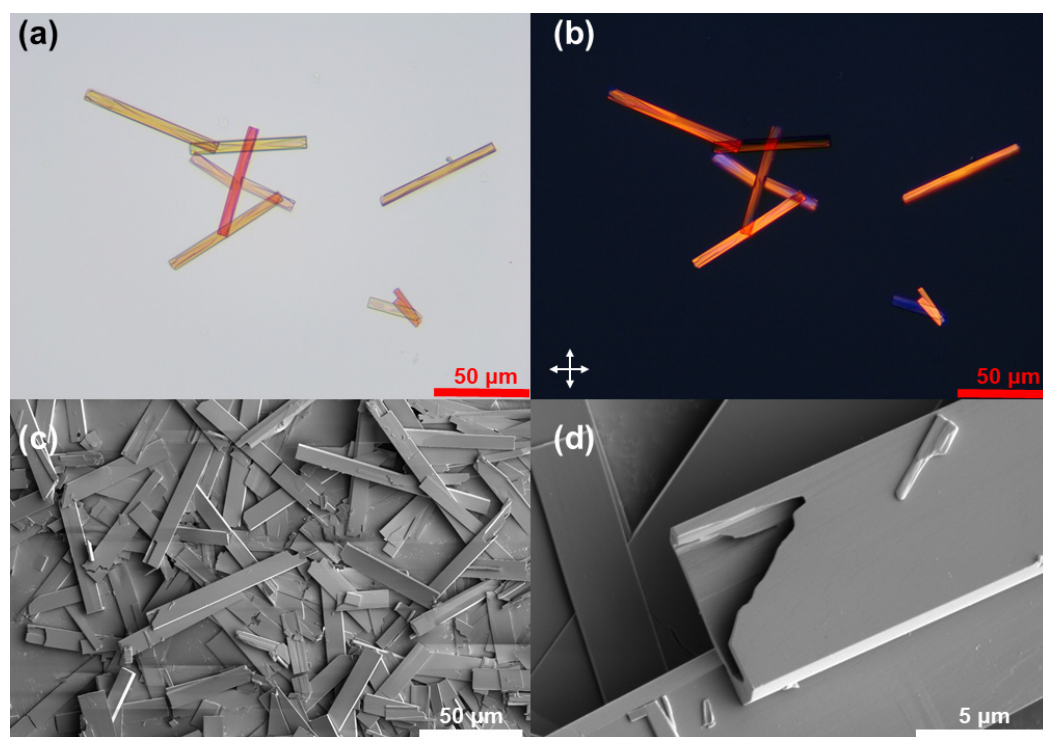| Temperature Surfactant	37 °C	47 °C	57 °C
SDS	Solid	Solid	Solid
BS12	Solid	Obvious hollow cavities	Obscure hollow structures

Figure 2. (**a**) The optical microscopy image of APE-TCNB hollow cocrystals; (**b**) the cross-polarized microscope image of APE-TCNB hollow cocrystals; (**c**) the SEM image of APE-TCNB hollow cocrystals; (**d**) the SEM image of a fractured APE-TCNB hollow cocrystal shows the interior structure.
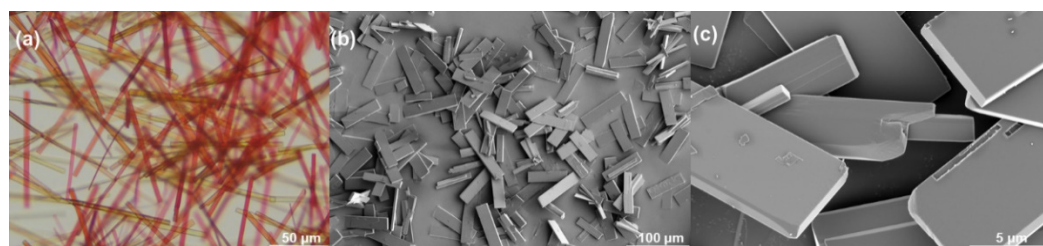

Figure 3. (**a**) Optical microscopy image of APE-TCNB solid cocrystals grown in SDS; (**b**) the SEM image of APE-TCNB solid cocrystals; (**c**) the SEM image of a fractured APE-TCNB solid cocrystal shows the interior structure.

First, we measured the UV-Vis absorption spectroscopy of these microcrystals to verify the formation of cocrystals. As shown in Figure 4a, the UV-Vis absorption spectra of APE and TCNB in organic solvent (DMF) exhibited very different absorption features. The APE showed a typical anthracene derivative character and mainly had two absorbance bands. The narrow high absorption band that peaks at approximately 280 nm is associated with the $S_0 \rightarrow S_2$ transition, and the broad short absorption band that is from 325 nm to 450 nm corresponds to the $S_0 \rightarrow S_1$ transition. In contrast, the UV-Vis absorption spectrum of TCNB solution has a short absorption band that peaks at approximately 320 nm, from 300 to 340 nm, corresponding to the $S_0 \rightarrow S_1$ transition. In the meantime, we measured the UV-Vis absorption spectrum of TCNB and APE with the same concentration in a DMF solution (Figure 4a, blue trace). However, no new absorption band could be observed, indicating APE and TCNB molecules cannot form effective CT interactions when they dissolve in solution. Then, we investigated the UV-Vis absorption spectrum of APE-TCNB hollow microcrystals suspended in pure water. As shown in Figure 4b, the prepared microcrystal suspension in pure water displayed a combination feature of APE and TCNB molecules. A prominent absorption band was observed at approximately 275 nm, and a

shorter absorption band was found from about 330 nm to 420 nm. These two absorption bands are from the absorption features of APE and TCNB molecules. Moreover, a new broad absorption band was observed from approximately 480 nm to 620 nm. The new peak indicated strong CT interactions between APE and TCNB molecules, as this absorption band was not found in either APE or TCNB crystals suspended in pure water. We also measured the infrared (IR) spectra of the solid-state APE, TCNB, and APE-TCNB cocrystals. As shown in Figure 4c, there are new peaks from 2766.5 cm^{-1} to 2992.6 cm^{-1} in the APE-TCNB samples as compared with the APE and TCNB solids, which suggests there are intermolecular interactions between the APE and TCNB molecules in the APE-TCNB cocrystal. Moreover, the IR peak associated with the pyridine ring in the APE molecule shifts from 1593.4 cm^{-1} to 1598.7 cm^{-1}, and the peak associated with the cyano groups in the TCNB molecule shifts from 2244.2 cm^{-1} to 2242.4 cm^{-1}, suggesting the CT interactions have been built in the APE-TCNB molecules. In addition, time-resolved fluorescence spectroscopy was conducted to investigate the fluorescence lifetime in the cocrystals. As shown in Figure 4d, the fluorescence decay of the APE powders suspended in water shows a single-exponential decay with a lifetime of about 0.93 ns, while the fluorescence decay of the APE-TCNB cocrystals in water showed a slightly longer lifetime of about 0.95 ns. We speculated that the CT interactions might delay the cocrystal lifetime. As a result, the APE and TCNB molecules have established stable CT interactions in the prepared microcrystals based on these measurements.
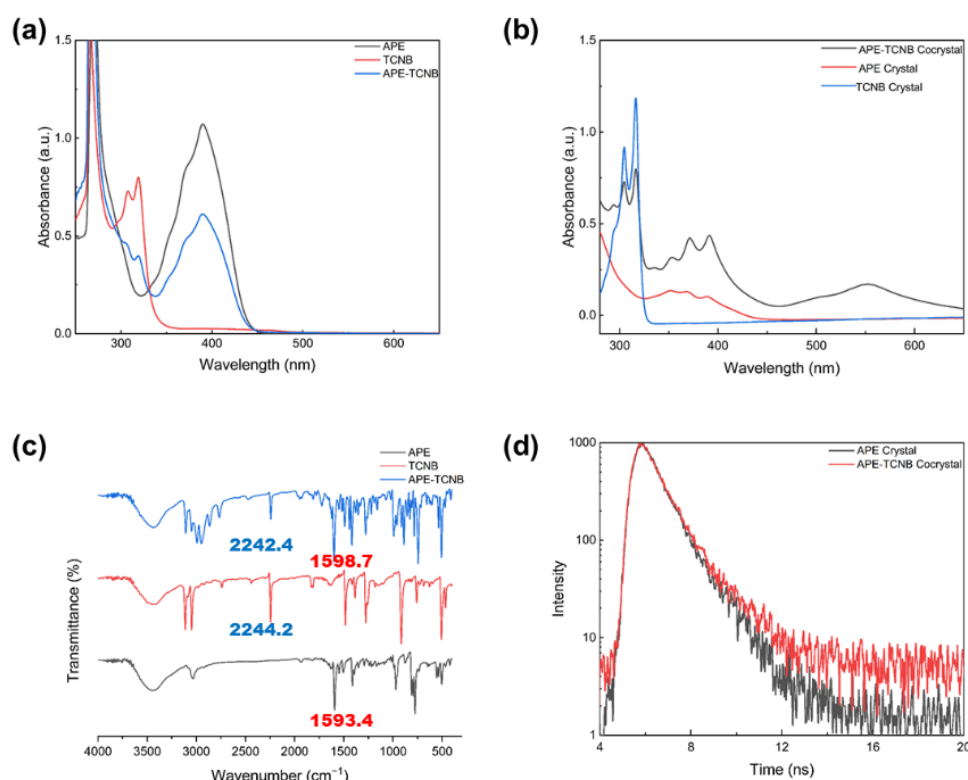

Figure 4. (**a**) UV-Vis absorption spectra of APE, TCNB, and APE-TCNB with equimolar concentrations in DMF solutions ([APE] = 1.0 × 10^{-5} M, [TCNB] = 1.0 × 10^{-5} M); (**b**) UV-Vis absorption spectra of APE-TCNB cocrystals, APE crystals, and TCNB crystals suspended in pure water; (**c**) IR spectra of APE, TCNB; and APE-TCNB powder; (**d**) time-resolved fluorescence decay spectra of APE solids and APE-TCNB cocrystals (both solids suspended in pure water).

We then used powder X-ray diffraction (PXRD) measurements to determine the molecular orientation in the APE-TCNB hollow microcrystals (Figure 5). The microcrystals were rinsed with sufficient Milli-Q water (18.2 mΩ/cm) to remove residue surfactants, and then were filtered out onto a commercial anodic alumina oxide template for drying at 50 °C for

24 h before PXRD measurements. Narrow and intense diffraction peaks at $2\theta = 10.22°$ and $2\theta = 15.36°$ were observed in the PXRD pattern, associated with the (004) and (006) Miller planes. The (004) and (006) Miller planes, which were parallel to the (001) Miller plane, were b oth expected to be perpendicular to the surface normal of APE-TCNB hollow microcrystals and the crystallographic *a*-axis (Figure 5c). We estimated the distance between the aromatic rings of the APE and TCNB molecules based on the single crystal structure and found the average distance was around 3.740 Å, showing relatively strong π–π stacking interactions (Figure S5a). Moreover, the abundant hydrogen bonds among the APE and TCNB molecules help stabilize the crystal structure (Figure S5b). The strong intermolecular CT and π–π interactions between APE and TCNB molecules facilitate effective assembly along the crystallographic *a*-axis. The cross-polarized microscope characterization also confirmed the high crystallinity and interior chamber structures of the APE-TCNB hollow microcrystals (Figures 2b and 5c).
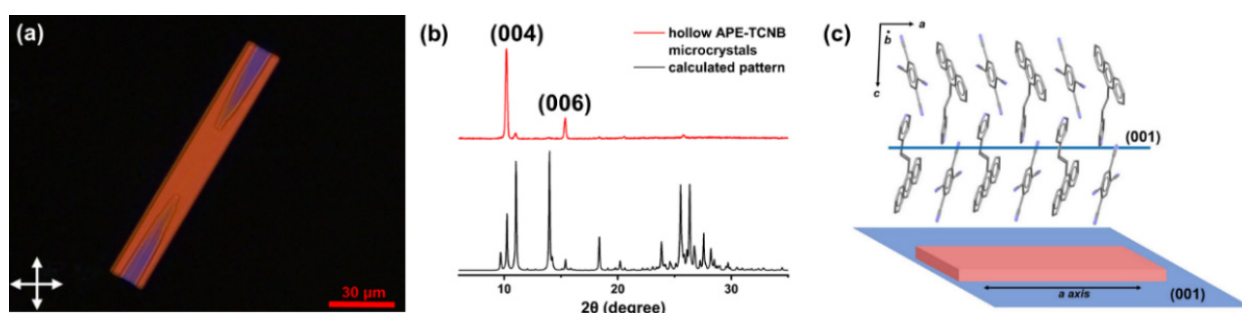

Figure 5. (**a**) The cross-polarized microscopy image of an APE-TCNB hollow cocrystal; (**b**) PXRD patterns of APE-TCNB (red) hollow cocrystals lying horizontally on the surface and the calculated PXRD pattern of APE-TCNB (black); (**c**) Molecule packing motif in the APE-TCNB cocrystals that are along the crystallographic *a*-axis.

The optical and electron microscopic images both showed that the hollow chambers might be open to the exterior, and we found no evidence of DMF solvent or any surfactant incorporated in the hollow crystal lattice. The fluorescence microscopy images showed that all APE-TCNB hollow microcrystals with different sizes could emit bright red luminescence upon 405 nm illumination (Figure 6a,b). The luminescence spectrum of APE-TCNB hollow microcrystals suspended in pure water also exhibited intense luminescence. Then, we carefully measured the excitation and emission fluorescence spectroscopy of the APE crystals and APE-TCNB cocrystals suspended in water. As shown in Figure 6c, the proper excitation wavelength of the APE crystals was found from 300 to 420 nm, while the excitation wavelength of the APE-TCNB was more redshifted, from 400 to 600 nm. Therefore, we selected 360 nm for the APE solids and 450 nm for the APE-TCNB cocrystals as excitation wavelength. As shown in Figure 6d, a broad emission band peaked at about 650 nm was observed in the APE-TCNB cocrystals and the emission band extended to the near-infrared region (~800 nm) (excited at 450 nm). In comparison, the emission band of the APE crystals suspended in pure water peaked at about 500 nm (excited at 360 nm). As a result, it revealed strong CT interactions between APE and TCNB molecules when the APE-TCNB cocrystals formed. The microcrystals were stable and still emitted bright photoluminescence after being stored in water for over 5 months. This is because of the high melting point of the APE-TCNB cocrystals (~216 °C), allowing long time storage under an ambient environment. Moreover, the APE-TCNB microcrystal stayed intact after 30 min intense sonication, which suggests the crystals have superior stability than other classical cocrystals (Figure 7a,b) [37].
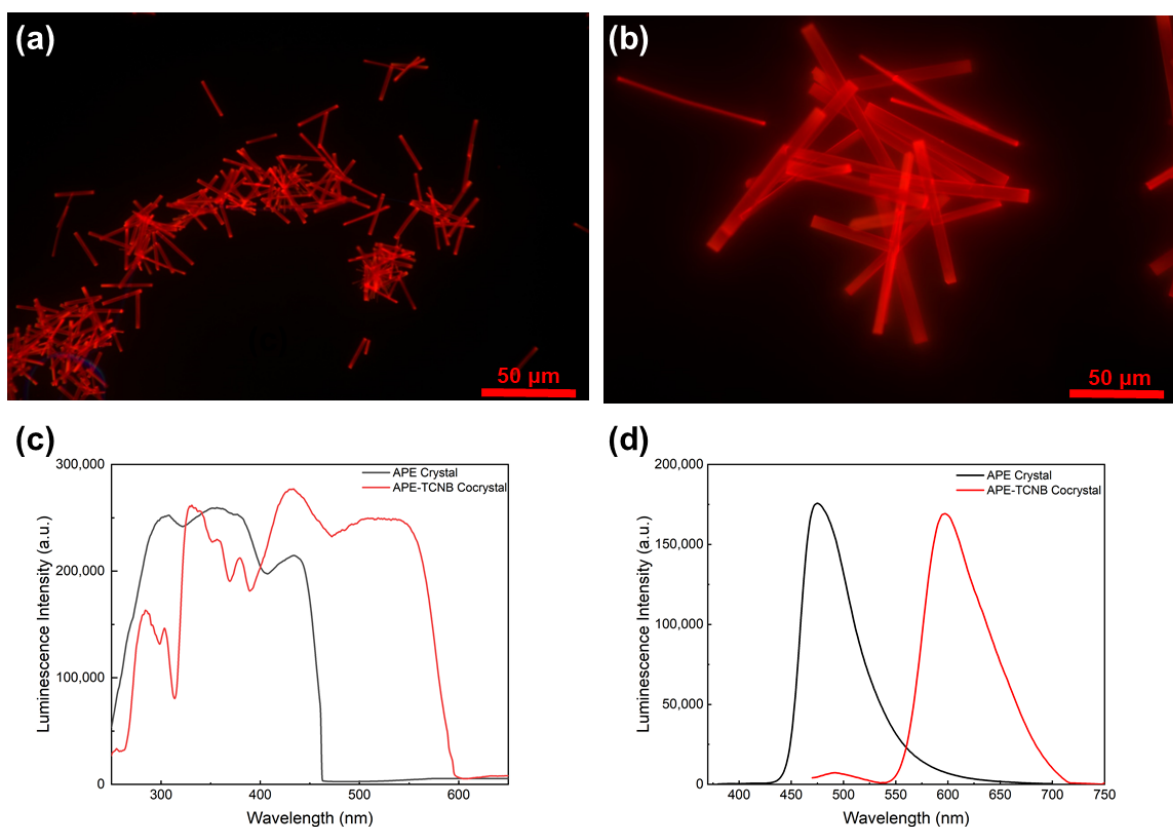
Figure 6. (**a**,**b**) Fluorescence microscopy images of the APE-TCNB cocrystals with different sizes illuminated by 405 nm light; (**c**) fluorescence excitation spectra of APE crystals and APE-TCNB cocrystals (emission at 650 nm); (**d**) fluorescence emission spectra of APE crystals (excited at 360 nm) and APE-TCNB cocrystals (excited at 450 nm).
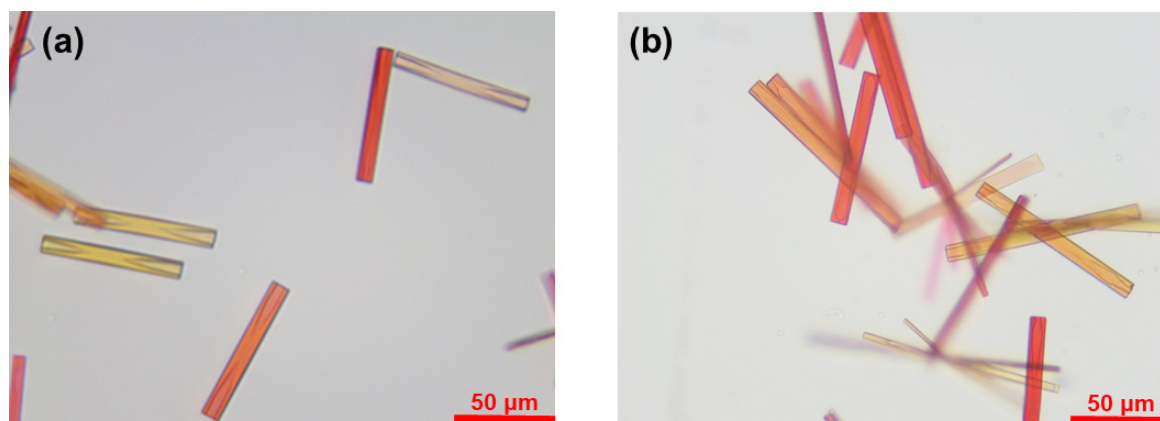

Figure 7. Optical microscopy images of APE-TCNB hollow cocrystals before (**a**) and after (**b**) 30 min intense sonication.

Although the mechanism of formation of hollow crystals is not fully illustrated, previous studies in the literature have shown that surfactants may contribute to the formation of crystal cavities [37–42]. In an aqueous surfactant solution, the surfactant micelles that contain acceptor and donor molecules will slowly diffuse and allow the cocrystal to precipitate out in a gradient way as the concentrations of donor and acceptor molecules gradually decrease as the growth proceeds. This process also causes a non-equilibrium growth condition, facilitating a faster growth rate at the crystal edges. In addition, the strong π–π intermolecular interactions along the crystallographic *a*-axis could promote rapid crystal growth in this direction. As a result, the molecules will rapidly crystallize along the outer

edges of the crystal along the *a*-axis, leading to the formation of tubular crystal structures. We found that the tubular structure formation must involve the participation of BS12 surfactants. We only found solid microrods in pure water or SDS aqueous solutions. In pure water or lower surfactant concentration solutions, solid rectangular microrods were formed. In the meantime, molecules must be contained in the surfactant micelles before mixing. If the APE and TCNB were mixed in DMF before injection to surfactant solutions, solid acicular crystals were found, similar to the traditional way of preparing bulk APE-TCNB crystals for single-crystal structure determination.

4. Conclusions

In summary, we have synthesized a new molecule APE that could be used as a donor molecular in fabricating CT cocrystals based on the anthracene framework and pyridine group. APE-TCNB hollow microcrystals that consist of metric twined cavities were prepared via a surfactant-mediated self-assembly method. The hollow microcrystals possess high crystallinity, and the crystal size can be qualitatively regulated by tuning the crystal growth conditions, such as mixing time, incubation temperature, surfactant, and crystal growth time. The crystal interior chamber structure is mainly ascribed to a comprehensive effect of CT interactions, π–π interactions between molecules, and non-equilibrium growth conditions caused by surfactant during the self-assembly. The APE-TCNB hollow microcrystals are very stable and can emit bright red luminescence that extends to the near-infrared region. These cocrystals with unique tubular structures can be potentially used in pharmaceutical areas, such as drug storage and delivery. Our results provide a facile way to fabricate cocrystals with complicated topology and broaden the potential application of organic cocrystals.

References

1. Wang, C.; Dong, H.; Jiang, L.; Hu, W. Organic semiconductor crystals. *Chem. Soc. Rev.* **2018**, *47*, 422–500. [CrossRef] [PubMed]
2. Yu, P.; Zhen, Y.; Dong, H.; Hu, W. Crystal engineering of organic optoelectronic materials. *Chem* **2019**, *5*, 2814–2853. [CrossRef]
3. Qiu, S.; Zhang, Z.; Wu, Y.; Tong, F.; Chen, K.; Liu, G.; Zhang, L.; Wang, Z.; Qu, D.-H.; Tian, H. Vibratile dihydrophenazines with controllable luminescence enabled by precise regulation of π-conjugated wings. *CCS Chem.* **2022**, *4*, 2344–2353. [CrossRef]
4. Naumov, P.; Chizhik, S.; Panda, M.K.; Nath, N.K.; Boldyreva, E. Mechanically responsive molecular crystals. *Chem. Rev.* **2015**, *115*, 12440–12490. [CrossRef] [PubMed]

5. Tong, F.; Qu, D.-H. Engineering shapes and sizes of molecular crystals to achieve versatile photomechanical behaviors. *Langmuir* **2022**, *38*, 4793–4801. [CrossRef]

6. Kitagawa, D.; Bardeen, C.J.; Kobatake, S. Symmetry breaking and photomechanical behavior of photochromic organic crystals. *Symmetry* **2020**, *12*, 1478. [CrossRef]

7. Wang, J.; Wu, X.; Pan, J.; Feng, T.; Wu, D.; Zhang, X.; Yang, B.; Zhang, X.; Jie, J. Graphene-quantum-dots-induced centimeter-sized growth of monolayer organic crystals for high-performance transistors. *Adv. Mater.* **2020**, *32*, 2003315. [CrossRef]

8. Karunatilaka, C.; Bučar, D.K.; Ditzler, L.R.; Friščić, T.; Swenson, D.C.; MacGillivray, L.R.; Tivanski, A.V. Softening and hardening of macro-and nano-sized organic cocrystals in a single-crystal transformation. *Angew. Chem. Int. Ed.* **2011**, *50*, 8642–8646. [CrossRef]

9. Shtukenberg, A.G.; Punin, Y.O.; Gujral, A.; Kahr, B. Growth actuated bending and twisting of single crystals. *Angew. Chem. Int. Ed.* **2014**, *53*, 672–699. [CrossRef]

10. Zhang, X.; Dong, C.; Zapien, J.A.; Ismathullakhan, S.; Kang, Z.; Jie, J.; Zhang, X.; Chang, J.C.; Lee, C.-S.; Lee, S.-T. Polyhedral organic microcrystals: From cubes to rhombic dodecahedra. *Angew. Chem. Int. Ed.* **2009**, *48*, 9121–9123. [CrossRef]

11. Lei, Y.; Liao, Q.; Fu, H.; Yao, J. Phase- and shape-controlled synthesis of single crystalline perylene nanosheets and its optical properties. *J. Phys. Chem. C* **2009**, *113*, 10038–10043. [CrossRef]

12. Lovette, M.A.; Browning, A.R.; Griffin, D.W.; Sizemore, J.P.; Snyder, R.C.; Doherty, M.F. Crystal shape engineering. *Ind. Eng. Chem. Res.* **2008**, *47*, 9812–9833. [CrossRef]

13. Shtukenberg, A.G.; Ward, M.D.; Kahr, B. Crystal growth with macromolecular additives. *Chem. Rev.* **2017**, *117*, 14042–14090. [CrossRef] [PubMed]

14. Darkins, R.; McPherson, I.J.; Ford, I.J.; Duffy, D.M.; Unwin, P.R. Critical step length as an indicator of surface supersaturation during crystal growth from solution. *Cryst. Growth Des.* **2022**, *22*, 982–986. [CrossRef] [PubMed]

15. Suzuki, D.; Nakabayashi, S.; Yoshikawa, H.Y. Control of organic crystal shape by femtosecond laser ablation. *Cryst. Growth Des.* **2018**, *18*, 4829–4833. [CrossRef]

16. Vaghasiya, J.V.; Sonigara, K.K.; Beuvier, T.; Gibaud, A.; Soni, S.S. Iodine induced 1-D lamellar self assembly in organic ionic crystals for solid state dye sensitized solar cells. *Nanoscale* **2017**, *9*, 15949–15957. [CrossRef]

17. Zhu, W.; Zheng, R.; Fu, X.; Fu, H.; Shi, Q.; Zhen, Y.; Dong, H.; Hu, W. Revealing the charge-transfer interactions in self-assembled organic cocrystals: Two-dimensional photonic applications. *Angew. Chem. Int. Ed.* **2015**, *54*, 6785–6789. [CrossRef]

18. Zhang, F.; Gu, D.; Yu, T.; Zhang, F.; Xie, S.; Zhang, L.; Deng, Y.; Wan, Y.; Tu, B.; Zhao, D. Mesoporous carbon single-crystals from organic-organic self-assembly. *J. Am. Chem. Soc.* **2007**, *129*, 7746–7747. [CrossRef]

19. Tong, F.; Xu, W.; Al-Haidar, M.; Kitagawa, D.; Al-Kaysi, R.O.; Bardeen, C.J. Photomechanically induced magnetic field response by controlling molecular orientation in 9-methylanthracene microcrystals. *Angew. Chem. Int. Ed.* **2018**, *57*, 7080–7084. [CrossRef]

20. Tong, F.; Kitagawa, D.; Bushnak, I.; Al-Kaysi, R.O.; Bardeen, C.J. Light-powered autonomous flagella-like motion of molecular crystal microwires. *Angew. Chem. Int. Ed.* **2021**, *60*, 2414–2423. [CrossRef]

21. Tong, F.; Al-Haidar, M.; Zhu, L.; Al-Kaysi, R.O.; Bardeen, C.J. Photoinduced peeling of molecular crystals. *Chem. Commun.* **2019**, *55*, 3709–3712. [CrossRef] [PubMed]

22. Al-Kaysi, R.O.; Tong, F.; Al-Haidar, M.; Zhu, L.; Bardeen, C.J. Highly branched photomechanical crystals. *Chem. Commun.* **2017**, *53*, 2622–2625. [CrossRef] [PubMed]

23. Hu, J.-S.; Guo, Y.-G.; Liang, H.-P.; Wan, L.-J.; Jiang, L. Three-dimensional self-organization of supramolecular self-assembled porphyrin hollow hexagonal nanoprisms. *J. Am. Chem. Soc.* **2005**, *127*, 17090–17095. [CrossRef] [PubMed]

24. Xu, T.-Y.; Tong, F.; Xu, H.; Wang, M.-Q.; Tian, H.; Qu, D.-H. Engineering photomechanical molecular crystals to achieve extraordinary expansion based on solid-state [2 + 2] photocycloaddition. *J. Am. Chem. Soc.* **2022**, *144*, 6278–6290. [CrossRef]

25. Nagai, A.; Nishimura, R.; Hattori, Y.; Hatano, E.; Fujimoto, A.; Morimoto, M.; Yasuda, N.; Kamada, K.; Sotome, H.; Miyasaka, H. Molecular crystalline capsules that release their contents by light. *Chem. Sci.* **2021**, *12*, 11585–11592. [CrossRef] [PubMed]

26. Isobe, M.; Kitagawa, D.; Kobatake, S. Effect of substrate surfaces for crystal growth of a photochromic diarylethene by sublimation. *Cryst. Growth Des.* **2022**, *22*, 5489–5496. [CrossRef]

27. Zhang, J.; Xu, W.; Sheng, P.; Zhao, G.; Zhu, D. Organic donor–acceptor complexes as novel organic semiconductors. *Acc. Chem. Res.* **2017**, *50*, 1654–1662. [CrossRef]

28. Sun, L.; Wang, Y.; Yang, F.; Zhang, X.; Hu, W. Cocrystal engineering: A collaborative strategy toward functional materials. *Adv. Mater.* **2019**, *31*, 1902328. [CrossRef]

29. Bond, A.D. What is a co-crystal? *CrystEngComm* **2007**, *9*, 833–834. [CrossRef]

30. Al-Kaysi, R.O.; Müller, A.M.; Frisbee, R.J.; Bardeen, C.J. Formation of cocrystal nanorods by solid-state reaction of tetracyanobenzene in 9-methylanthracene molecular crystal nanorods. *Cryst. Growth Des.* **2009**, *9*, 1780–1785. [CrossRef]

31. Deibel, C.; Strobel, T.; Dyakonov, V. Role of the charge transfer state in organic donor–acceptor solar cells. *Adv. Mater.* **2010**, *22*, 4097–4111. [CrossRef] [PubMed]

32. Mukherjee, A.; Rogers, R.D.; Myerson, A. Cocrystal formation by ionic liquid-assisted grinding: Case study with cocrystals of caffeine. *CrystEngComm* **2018**, *20*, 3817–3821. [CrossRef]

33. Stahly, G.P. A survey of cocrystals reported prior to 2000. *Cryst. Growth Des.* **2009**, *9*, 4212–4229. [CrossRef]

34. Karimi-Jafari, M.; Padrela, L.; Walker, G.M.; Croker, D.M. Creating cocrystals: A review of pharmaceutical cocrystal preparation routes and applications. *Cryst. Growth Des.* **2018**, *18*, 6370–6387. [CrossRef]

35. Huang, Y.; Wang, Z.; Chen, Z.; Zhang, Q. Organic cocrystals: Beyond electrical conductivities and field-effect transistors (FETs). *Angew. Chem. Int. Ed.* **2019**, *58*, 9696–9711. [CrossRef]
36. Yao, Z.; Zhang, M.; Wu, H.; Yang, L.; Li, R.; Wang, P. Donor/acceptor indenoperylene dye for highly efficient organic dye-sensitized solar cells. *J. Am. Chem. Soc.* **2015**, *137*, 3799–3802. [CrossRef]
37. Tong, F.; Li, W.; Li, Z.; Islam, I.; Al-Kaysi, R.O.; Bardeen, C.J. Molecular crystal microcapsules: Formation of sealed hollow chambers via surfactant-mediated growth. *Angew. Chem. Int. Ed.* **2020**, *59*, 23035–23039. [CrossRef]
38. Bakshi, M.S. How surfactants control crystal growth of nanomaterials. *Cryst. Growth Des.* **2016**, *16*, 1104–1133. [CrossRef]
39. Karanjkar, P.U.; Lee, J.W.; Morris, J.F. Surfactant effects on hydrate crystallization at the water-oil interface: Hollow-conical crystals. *Cryst. Growth Des.* **2012**, *12*, 3817–3824. [CrossRef]
40. Zhou, S.W.; Tong, F.; Chen, M.; Gu, R.; Shi, C.Y.; Yu, C.Y.; Zhang, Q.; Qu, D.H. Self-evolution of high mechanical strength dry-network polythiourethane thermosets into neat macroscopic hollow structures. *Angew. Chem. Int. Ed.* **2022**, *61*, e202117195.
41. Wang, Q.; Zhang, Q.; Zhang, Q.-W.; Li, X.; Zhao, C.-X.; Xu, T.-Y.; Qu, D.-H.; Tian, H. Color-tunable single-fluorophore supramolecular system with assembly-encoded emission. *Nat. Commun.* **2020**, *11*, 158. [CrossRef] [PubMed]
42. Iwanaga, H.; Shibata, N. Growth mechanism of hollow ZnO crystals from ZnSe. *J. Cryst. Growth* **1974**, *24*, 357–361. [CrossRef]